Mühendislik Bilimleri ve Tasarım Dergisi
13(1), 185-201, 2025
e-ISSN: 1308-6693

Journal of Engineering Sciences and Design
DOI: 10.21923/jesd.1510194

Araştırma Makalesi
Research Article

GÖMÜLÜ SABİT MIKNATISLI SENKRON MOTOR SÜRÜCÜ TASARIMI: KLİMA SİSTEMLERİNDE KULLANILAN FAN YÜKÜ UYGULAMASI

Buğra ER[1], Okan BİNGÖL[2*]

[1] KORMAS, TOSB, Kocaeli, Türkiye
[2] Isparta Uygulamalı Bilimler Üniversitesi, Mühendislik Fakültesi, Elektrik Elektronik Mühendisliği Bölümü, Isparta, Türkiye

Anahtar Kelimeler

Gömülü SMSM, Sensörsüz Kontrol, Zıt-EMK Gözlemcisi, Motor Sürücü Tasarımı.

Öz

Gömülü sabit mıknatıslı senkron motorlar (GSMSM), verimlerinin yüksek olması, yüksek güç yoğunluğuna sahip olmaları, düşük bakım gerektirmeleri, hızlı tepki süreleri ve yüksek dinamik performansına sahip olmalarından dolayı fan, pompa ve iklimlendirme gibi endüstriyel uygulamalarda son yıllarda yaygın olarak kullanılmaya başlamıştır. Bu motorların kontrolü için gerçek zamanlı konum ve hız bilgisi sensörlerden elde edilmektedir. Sensörlerin maliyeti, ağırlıkları ve hacimleri, güvenirliği ve dayanımları gibi durumlardan dolayı gömülü SMSM larda sensörsüz kontrol yöntemleri araştırmacılar için ilgi odağı haline gelmiştir.

Bu çalışmada, araçlardaki klima sistemlerinde kullanılmak üzere gömülü sabit mıknatıslı senkron motorların performansını ve verimini artırmak için hem motor sürücü tasarımı hem de motorun sensörsüz kontrolüne ait uygulama gerçekleştirilmiştir. Gömülü SMSM' un hız kontrolünde alan yönlendirmeli kontrol yöntemi kullanılmıştır. Düşük maliyet, dayanıklık ve iyi performans elde edebilmek için Luenberger tipi sensörsüz kontrol yöntemi kullanılmıştır. Akım ve gerilim bilgileri kullanılarak Zıt-EMK yöntemi ile gömülü SMSM' un rotor konumu ve hız bilgisi elde edilmiştir. Gömülü SMSM klasik iki-seviyeli inverter tarafından beslenmiştir. İnverterdeki yarıiletken güç anahtarların kontrolü için uzay vektör darbe genişlik modülasyon tekniği kullanılmıştır. Deneysel sonuçlar, önerilen sensörsüz kontrol tekniğinin gömülü SMSM' ları için endüstriyel fan uygulamalarında yüksek performans gösterdiğini doğrulamaktadır.

INTERIOR PERMANENT MAGNET SYNCHRONOUS MOTOR DRIVER DESIGN: FAN LOAD APPLICATION USED IN AIR CONDITIONING SYSTEMS

Keywords

Interior PMSM, Sensorless Control, Back-Emf Observer, Motor Drive Design.

Abstract

Interior permanent magnet synchronous motors (IPMSMs) have gained significant popularity for industrial applications such as fans, pumps, and air conditioning system, owing to their high efficiency, power density, low maintenance, quick response, and dynamic performance. For controlling these motors, real-time position and speed data are typically obtained via sensors. However, the associated costs, added weight, increased volume, and potential reliability issues have driven interest in sensorless control methods for IPMSMs.

This study aims to enhance the performance and efficiency of an IPMSM designed for automotive air conditioning systems, in which involves the implementation of both motor driver design and sensorless control. The field-oriented control (FOC) method is employed for the speed control of the IPMSM. To maintain low costs and ensure durability and high performance, a Luenberger-type sensorless control method is used. The rotor position and speed information are derived using the Back-EMF method, based on current and voltage data. The IPMSM is driven by a conventional two-level inverter, with the SVPWM technique managing the semiconductor power switches. Experimental results confirm that proposed sensorless control technique of IPMSMs conducted the high performance in industrial fan applications.

Alıntı / Cite

ER, B., Bingöl, O., (2025). Interior Permanent Magnet Synchronous Motor Driver Design: Fan Load Application Used in Air Conditioning Systems, Journal of Engineering Sciences and Design, 13(1), 185-201.

Yazar Kimliği / Author ID (ORCID Number)
B. Er, 0000-0002-3982-5654
O. Bingöl, 0000-0001-9817-7266

Makale Süreci / Article Process	
Başvuru Tarihi / Submission Date	03.07.2024
Revizyon Tarihi / Revision Date	04.10.2024
Kabul Tarihi / Accepted Date	08.01.2025
Yayım Tarihi / Published Date	20.03.2025

* İlgili yazar / Corresponding author: okanbingol@isparta.edu.tr, +90-246-214-67-57

INTERIOR PERMANENT MAGNET SYNCHRONOUS MOTOR DRIVER DESIGN: FAN LOAD APPLICATION USED IN AIR CONDİTİONİNG SYSTEMS

Buğra ER[1], Okan BINGÖL[2†]
[1] Kormas, TOSB, Kocaeli, Turkey
[2] Electrical-Electronics Engineering, Technology Faculty, Isparta University of Applied Sciences, Isparta, Turkey

Highlights

- Developed sensorless control for interior PMSMs using a back-EMF observer.
- Improved efficiency and dynamic response in motor drives.
- Validated through simulations and experimental setups.
- Reduced system cost and complexity in industrial applications.

Purpose and Scope

The aim of this study is to develop and validate sensorless control methods for permanent magnet synchronous motors (PMSMs), with a particular focus on a back-EMF observer-based technique. The scope encompasses the mathematical modeling, simulation, and experimental validation of these methods across different industrial applications.

Design/methodology/approach

This research employs a comprehensive methodology, beginning with the transformation of PMSM's three-phase (abc) system to a two-phase (dq) reference frame. A Luenberger observer-based back-EMF observer is designed and tested through simulations and experimental setups to estimate rotor position and speed without mechanical sensors.

Findings

The findings indicate that the proposed sensorless control strategies offer high efficiency, reduced torque ripple, and improved dynamic response compared to traditional sensor-based methods. The results validate the effectiveness of the back-EMF observer in various operational conditions.

Research limitations/implications

The research is limited to specific types of interior PMSMs and control hardware. Future studies should explore the application of these techniques to other motor types and configurations to enhance generalizability.

Practical implications

The implementation of sensorless control techniques can reduce the cost and complexity of motor drive systems, leading to more robust and maintenance-free industrial applications.

By improving the efficiency and reliability of motor control systems, the research contributes to energy savings and sustainability, benefiting industries and society at large.

Originality

This study offers a novel approach to interior PMSM control by integrating a back-EMF observer into sensorless FOC systems, providing a cost-effective and efficient alternative to traditional sensor-based methods.

† Corresponding author: okanbingol@isparta.edu.tr, +90-246-214-67-57

1. Introduction

Permanent magnet synchronous motors (PMSM), which combine the best features of conventional direct current and alternating current motors, are becoming increasingly popular in the AC adjustable drive field due to the quick advancements in control technology, power electronics, converters, microprocessors, sensors, and permanent magnetic materials (Krishnan, 1987; Volpato et al., 2021; Zhang, 2022; Saleh et al., 2023). As PMSMs' rotors are made of magnets rather of windings, they may obtain the excitation flux without the need for an external excitation source. They also have a simpler construction than the typical motors used in the industry because they don't include parts like brushes and collectors that are present in direct current motors (Aydoğmuş & Sunter, 2012; Wang et al., 2019; Saleh et al., 2023).
Permanent magnet synchronous motors (PMSMs) are widely used in a wide range of industrial applications where low-to-medium power positioning is required. Robotics, machine tools, healthcare, Heating, Ventilation & Air Conditioning (HVAC), home appliances, electric/hybrid cars, renewable energy systems, transportation, and the aerospace and defense sectors are some of these applications (Yan et al., 2019; Ullah et al., 2022). According to Krishnan (1987), Elmas and Ustun (2008), Song et al. (2016), Saleh et al. (2023), compact design, high torque-to-weight and torque-to-inertia ratios, high power factor, high efficiency, smooth torque at high and low speeds, quick acceleration and deceleration, low noise, low maintenance requirements, and no rotor losses are some of the benefits of PMSMs. Other benefits include these advantages.

For these doubly excited electric machines, the synchronous speed of rotation is determined by the number of poles on the motor and the frequency of voltage applied to the stator windings. In synchronous motors, the stator magnetic field is produced by a three-phase AC voltage source supplied to the stator windings, while the rotor magnetic field is produced by permanent magnets installed on the rotor (Aydoğmuş and Sunter, 2012).

The two types of PMSMs are identified by the placement of the permanent magnets on the rotor: Surface PMSMs (SPMSMs) and Interior PMSMs (IPMSMs). In SPMSMs, permanent magnets are placed on the rotor's exterior, whereas in IPMSMs, they are integrated into the rotor (Sen, 1990, Wang et al., 2019, Jung et al., 2023). SPMSMs and IPMSMs are more efficient than conventional motors because they use permanent magnets rather than rotor windings. IPMSMs have reluctance torque in addition to magnetic torque, which makes them more efficient than SPMSMs. The same magnetic volume is intended for both SPMSMs and IPMSMs. Despite having nearly identical stator structures to other motors, SPMSMs and IPMSMs are more expensive because their rotor structures are made of different materials. The permanent magnets in SPMSMs become dislodged due to large centrifugal forces applied at high speeds. Because stainless steel keeps the permanent magnets from moving under centrifugal forces, SPMSMs are more expensive than IPMSMs. As a result, in recent years, academics, scientists, and engineers have become increasingly interested in IPMSMs because of their reduced cost, strong starting torque, quick response times, and good dynamic performance (Murakami et al., 1999, Noguchi, 2007, Rahman et al., 2008, Genduso et al., 2010). The cross-sections of SPMSM and IPMSM motors are displayed in Figure 1.

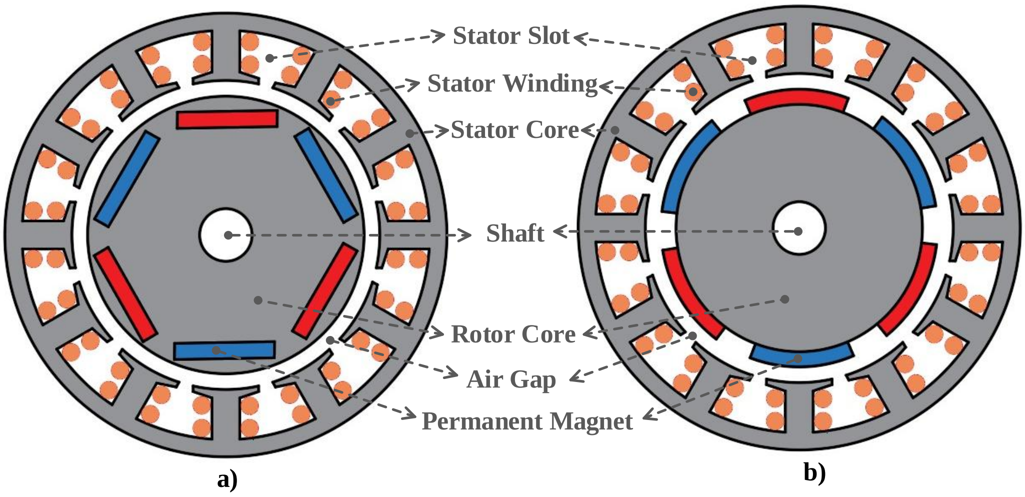

Figure 1. Cross-Sections Of Motors A) IPMSM B) SPMSM

One popular vector control method for permanent magnet synchronous motors (PMSMs) is the field-oriented control (FOC) method (Krishnan, 1987; Ullah et al., 2022; Zhang Z, 2022; Vidlak, 2022). To establish motor control, this method entails utilizing the d-q axis transformation to convert the three-phase motor equations into a two-dimensional vector plane (Sen, 1990; Güngör et al., 2010; Wang et al., 2019; Saleh et al., 2023).

Typically, sensors such as photoelectric encoders and Hall effect sensors are mounted on the rotor shaft to obtain real-time rotor position and speed information in PMSMs. However, the inclusion of these sensors adds complexity, cost, weight, and volume to the motor and driver system, while reducing reliability and robustness. To overcome these challenges, researchers have focused on developing sensorless control methods to achieve low-cost, durable, and high-performance PMSMs (Wang et al., 2019; Volpato et al., 2021; Genduso et al., 2010; Song et al., 2016; Zhang, 2022; Saleh et al., 2023). Sensorless control aims to derive rotor position and speed information from measured electrical quantities such as voltage and current (Piippo et al., 2009; Genduso et al., 2010). To get real-time rotor position and speed data in PMSMs, sensors like Hall effect sensors and photoelectric encoders are typically installed on the rotor shaft. Nevertheless, the motor and driver system's complexity, cost, weight, and volume are increased with the addition of these sensors, at the expense of their robustness and reliability. In order to address these issues and produce low-cost, long-lasting, and high-performing PMSMs, researchers have concentrated on creating sensorless control techniques (Wang et al., 2019; Volpato et al., 2021; Genduso et al., 2010; Song et al., 2016; Zhang, 2022; Saleh et al., 2023). By measuring electrical parameters like voltage and current, sensorless control seeks to extract information about the rotor's location and speed (Piippo et al., 2009; Genduso et al., 2010). Numerous sensorless control methods for PMSMs are extensively studied in the literature.

Two general approaches can be used for sensorless rotor position estimation in PMSMs (Song et al., 2016; Volpato et al., 2021). Among these is the saliency-based sensorless control approach, which works well at low speeds and determines position via motor reluctance through high-frequency injection (Zhang G. et al., 2017; Vidlak, 2022). Saliency-based techniques are further separated into two categories: fundamental PWM excitation-based (Zhang H. et al., 2020) and signal injection-based (Zhang X. et al., 2017). Some of the widely used methods are Zero Sequence Current Derivatives Measurements (Hind et al., 2017), Rotating Signal Injection (Kim et al., 2016), Pulsating Signal Injection (Luo, 2016), Zero Voltage Vector Injection (Wang G. et al., 2018), and Indirect Flux Detection by On-line Reactance Measurement (Schroedl, 1996).

The model-based sensorless control method, which computes the PMSM's flux or electromotive force in direct proportion to rotor position, is employed for high-speed ranges (Wang G. et al., 2019). Several notable techniques have been proposed (Aydoğmuş and Sunter, 2012; Ni et al., 2017; Wang G. et al., 2019; Volpato et al., 2021; Zhang Z, 2022). These include the Kalman Filter (Borsje et al., 2005), Extended Kalman Filter (Quang N. K., 2014), Luenberger Observer (Henwood et al., 2012), Sliding Mode Observer (Kim H. et al., 2011), Model Reference Adaptive Systems (Abo-Khalil et al., 2021), Artificial Neural Network-based Observer (Tan et al., 2021), and Fuzzy Logic Systems (Yan et al., 2019).

One popular sensorless control method for PMSMs is the Back EMF method (Genduso et al., 2010; Wang and Blaabjerg, 2012; Zhang Z, 2022; Vidlak, 2022). Using motor current and voltage data, this method determines the voltages induced in the stator windings by the magnets. Rotor position and speed data are then obtained (Wang Q. et al., 2019).

Reducing the harmonic components of voltage and current at voltage-fed inverters' output is essential in PMSM systems. These harmonics can be reduced by using a variety of PWM techniques at high switching frequencies (Liang et al., 2014; Bingol and Elmas, 2017). Due to its effective use of the input DC bus voltage, smaller switching losses, and fewer harmonic components in the output voltage, the Space Vector PWM approach has become more and more popular among them (Yan et al., 2019; Huang et al., 2023).

In this work is developed a sensorless control application for vehicle air conditioning systems using an interior permanent magnet synchronous motor (IPMSM). The IPMSM was selected because to its great dynamic performance, quick response times, high starting torque, and inexpensive cost. The IPMSM's speed was managed using the field-oriented control approach. A sensorless control approach of the Luenberger type was used to achieve low cost, durability, and good performance. The Back EMF technique was utilized to ascertain the IPMSM's rotor position and speed using current and voltage data. A traditional two-level inverter that used the SVPWM approach to regulate the inverter's semiconductor power switches provided power to the IPMSM.

There are seven sections in this research, starting with the introduction. The IPMSM's mathematical model is presented in Section 2. The control architecture of the sensorless FOC controller with the Luenberger-type Back EMF observer is explained in Section 3. The use of Space Vector PWM to regulate a traditional two-level inverter is described in Section 4. The PMSM driver's design is given in Section 5. The findings of the experiment are shown in Section 6. Conclusions are given in Section 7.

2. Mathematical Model

Mathematical models have been developed for the two-phase dq and three-phase abc systems in order to understand the field-oriented control of a PMSM (Sen, 1990; Güngör et al., 2010; Wang et al., 2019; Saleh et al., 2023). The analogous circuit for the stator windings of a three-phase, star-connected IPMSM is depicted in Figure 2. Figure 2 shows the induced back-EMF in the stator windings as e_a, e_b, and e_c.

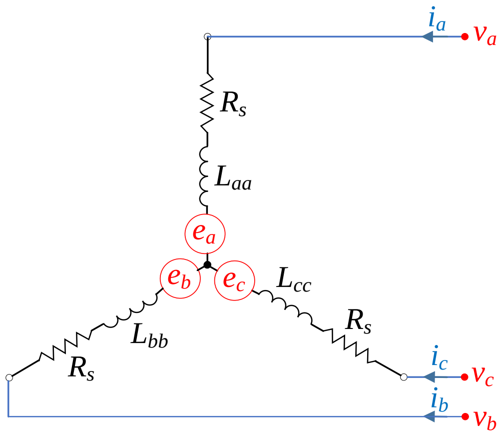

Figure 2. Three-Phase Equivalent Circuit Of IPMSM Stator Windings

In a three-phase, star-connected IPMSM with a rotor connected to a permanent magnet, the stator windings have a 120° phase difference, and the phase windings are assumed to be balanced. The stator voltages of the IPMSM in matrix form are shown in Equation 1 (Vidlak, 2022).

$$\begin{bmatrix} v_a \\ v_b \\ v_c \end{bmatrix} = \begin{bmatrix} R_a & 0 & 0 \\ 0 & R_b & 0 \\ 0 & 0 & R_c \end{bmatrix} \begin{bmatrix} i_a \\ i_b \\ i_c \end{bmatrix} + \frac{d}{dt} \begin{bmatrix} \psi_a \\ \psi_b \\ \psi_c \end{bmatrix} \quad (1)$$

The stator phase voltages in this case are v_a, v_b, and v_c; the stator winding resistances are $R_a = R_b = R_c = R_s$; the stator phase currents are i_a, i_b, and i_c; and the stator flux linkages are ψ_a, ψ_b,ψ_c.

$$\begin{bmatrix} \psi_a \\ \psi_b \\ \psi_c \end{bmatrix} = \begin{bmatrix} L_{aa} & L_{ab} & L_{ac} \\ L_{ba} & L_{bb} & L_{bc} \\ L_{ca} & L_{cb} & L_{cc} \end{bmatrix} \begin{bmatrix} i_a \\ i_b \\ i_c \end{bmatrix} + \psi_m \begin{bmatrix} \cos\theta_e \\ \cos(\theta_e - 2\pi/3) \\ \cos(\theta_e - 4\pi/3) \end{bmatrix} \quad (2)$$

L_{aa}, L_{bb}, L_{cc} represent the self-inductances of the phase windings, $L_{ab} = L_{ba}$, $L_{bc} = L_{cb}$ $L_{ac} = L_{ca}$ represent the mutual inductances between the phase windings, ψ_m is the magnetic flux of the permanent magnet, and θ_e is the electrical position of the rotor. By applying the Clarke and Park transformations to the three-phase voltages (Equation 1) and flux linkages (Equation 2), the dq reference frame is obtained.

$$\begin{bmatrix} v_d \\ v_q \end{bmatrix} = \begin{bmatrix} R_s & 0 \\ 0 & R_s \end{bmatrix} \begin{bmatrix} i_d \\ i_q \end{bmatrix} + \frac{d}{dt} \begin{bmatrix} \psi_d \\ \psi_q \end{bmatrix} + \omega_e \begin{bmatrix} -\psi_q \\ \psi_d \end{bmatrix} \quad (3)$$

Here, the stator voltage's dq components are represented by v_d and v_q. ω_e is the electrical angular speed of the rotor; ψ_q and ψ_d are the dq components of the equivalent magnetic flux; and i_d and i_q are the dq components of the stator current.

$$\begin{bmatrix} \psi_d \\ \psi_q \end{bmatrix} = \begin{bmatrix} L_d & 0 \\ 0 & L_q \end{bmatrix} \begin{bmatrix} i_d \\ i_q \end{bmatrix} + \psi_m \begin{bmatrix} 1 \\ 0 \end{bmatrix} \quad (4)$$

Here, L_d and L_q are the dq components of the synchronous inductance. Substituting the equivalent magnetic flux components ψ_q and ψ_d from Equation 4 into Equation 3 yields Equation 5.

$$\begin{bmatrix} v_d \\ v_q \end{bmatrix} = \begin{bmatrix} R_s & 0 \\ 0 & R_s \end{bmatrix} \begin{bmatrix} i_d \\ i_q \end{bmatrix} + \begin{bmatrix} L_d & 0 \\ 0 & L_q \end{bmatrix} \frac{d}{dt} \begin{bmatrix} i_d \\ i_q \end{bmatrix} + \omega_e \begin{bmatrix} -L_q \\ L_d \end{bmatrix} \begin{bmatrix} i_q \\ i_d \end{bmatrix} + \omega_e \psi_m \begin{bmatrix} 0 \\ 1 \end{bmatrix} \quad (5)$$

The electromagnetic torque is given by Equations 6 and 7.

$$T_e = \frac{3}{2}p[\psi_m i_q + (L_d - L_q)i_d i_q] \quad (6)$$

Here, p is the number of pole pairs.

$$T_e = J\frac{d}{dt}\omega_e + T_L + B\omega_e \quad (7)$$

Here, J is the moment of inertia, B is the coefficient friction, T is the electromechanical torque, T_L is the load torque, and p is the motor's pole count. The IPMSM parameters are displayed in Table 1.

Table 1. Parameters Of IPMSM.

Parameter	Value
Rated speed	3100 d/d
Rated power	180 W
Rated voltage	26 V
Rated current	7 A
Pole pairs	4
Stator resistance	0.0282124 Ω
Stator winding factor	0,866025
PM material	N35H

3. Sensorless FOC With Luenberger-Type Back-EMF Observer

Figure 3 shows the block design of the sensorless FOC with a back-EMF observer of the Luenberger type.

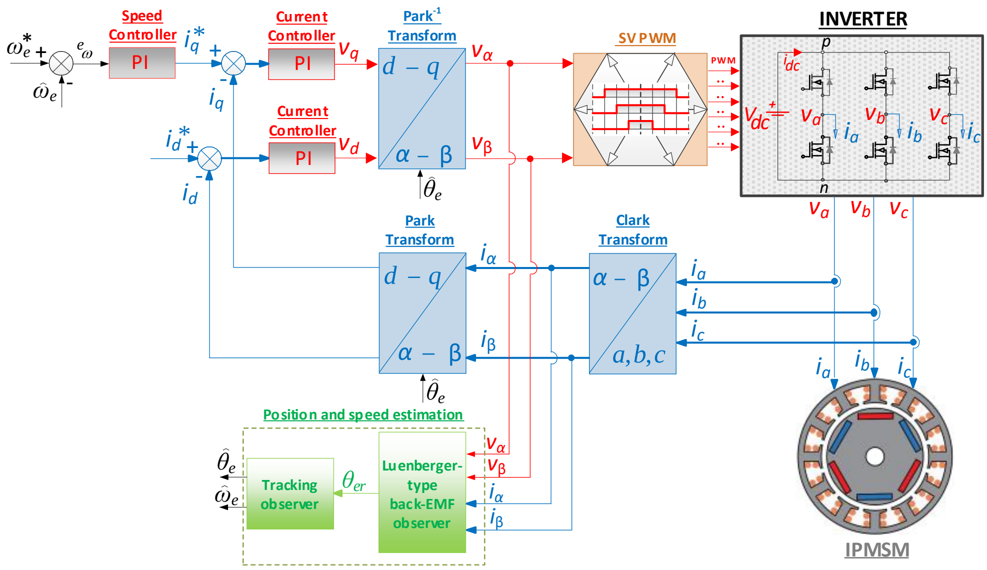

Figure 3. Block Diagram Of The Sensorless FOC Using A Back-EMF Observer Of The Luenberger Type

The saliency-based sensorless control approach is effective at low or zero speed ranges, but increases losses, torque ripples, and acoustic noise because of the injected signal. Furthermore, the maximum output voltage of the inverter may be limited by the injected signal at high operating speeds. Consequently, it is advised to only employ model-based techniques above a particular speed and to reserve the usage of injected signal-based approaches for low and zero-speed ranges (Wang G. et al., 2019). EMF and flow data can be directly computed in the model-based sensorless control method utilizing either open-loop or closed-loop techniques. Because of closed-loop estimation's high accuracy and resilience, it is recommended. For the purpose of estimating position and speed, accurate EMF or flux measurement is essential (Wang G. et al., 2019). EMF or flux can be measured when the observer error is close to zero, which enables precise position and speed calculation. In order to increase estimation accuracy, a position/speed observer is traditionally recommended. proportional-integral (PI) type

Luenberger observer can be used to force the position error signal to zero in order to get position/speed information (Wang G. et al., 2019).

The sensorless method's main goal is to calculate the back-EMF voltage in order to determine the rotor position. It is possible to rewrite Equation 5 as Equation 6.

$$\begin{bmatrix} v_d \\ v_q \end{bmatrix} = \begin{bmatrix} R_s + L_d s & -\omega_e L_q \\ \omega_e L_d s & R_s + L_q s \end{bmatrix} \begin{bmatrix} i_d \\ i_q \end{bmatrix} + \omega_e \psi_m \begin{bmatrix} 0 \\ 1 \end{bmatrix} \quad (8)$$

In this equation, "s" signifies the Laplace operator. The mathematical model in the dq reference frame alone cannot determine the rotor position. To estimate the position error θ_{er} , the γδ reference frame, which lags behind the dq reference frame, is obtained. The reference frames are shown in Figure 4.

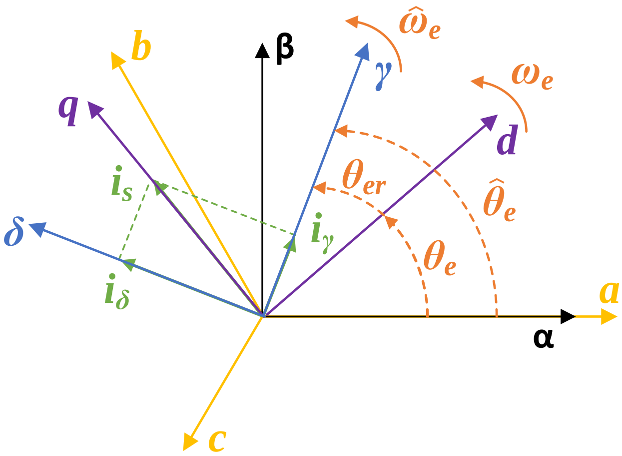

Figure 4. Reference Frames Of IPMSM

Equation 8 can be rearranged as shown in Equation 9.

$$\begin{bmatrix} v_d \\ v_q \end{bmatrix} = \begin{bmatrix} R_s + L_d s & -\omega_e L_q \\ \omega_e L_d s & R_s + L_q s \end{bmatrix} \begin{bmatrix} i_d \\ i_q \end{bmatrix} + E_{ex} \begin{bmatrix} 0 \\ 1 \end{bmatrix} \quad (9)$$

Equation 10 defines E_{ex}, as the extended EMF (EEMF) term.

$$E_{ex} = \omega_e\left[(L_d - L_q)i_d + \psi_m\right] - (L_d - L_q)si_q \quad (10)$$

The voltage equations from Equation 9 are converted from the dq reference frame to the γδ reference frame, as shown in Equation 11.

$$\begin{bmatrix} v_\gamma \\ v_\delta \end{bmatrix} = \begin{bmatrix} R_s + L_d s & -\omega_e L_q \\ \omega_e L_d s & R_s + L_q s \end{bmatrix} \begin{bmatrix} i_\gamma \\ i_\delta \end{bmatrix} + \begin{bmatrix} e_\gamma \\ e_\delta \end{bmatrix} \quad (11)$$

Here, e_γ and e_δ are the components of the EEMF in the γδ reference frame.

$$\begin{bmatrix} e_\gamma \\ e_\delta \end{bmatrix} = E_{ex} \begin{bmatrix} -\sin(\theta_{er}) \\ \cos(\theta_{er}) \end{bmatrix} + (\hat{\omega}_e - \omega_e)L_d \begin{bmatrix} -i_\delta \\ i_\gamma \end{bmatrix} \quad (12)$$

Here, $\hat{\omega}_e$ is the estimated rotor speed. The second portion of Equation 12 can be disregarded under the steady-state condition if there is no inaccuracy between the estimated and real rotor speeds, $\hat{\omega}_e$ and ω_e, respectively. The estimated γδ components of the EEMF can be expressed as in Equation 13.

Here, $\hat{\omega}_e$ represents the estimated rotor speed. Under steady-state conditions, the second term in Equation 12 can be disregarded, assuming the error between the estimated rotor speed $\hat{\omega}_e$ and the actual rotor speed ω_e is negligible. Thus, the estimated γδ components of the back-EMF can be written as in Equation 13.

$$\begin{bmatrix}\hat{e}_\gamma\\ \hat{e}_\delta\end{bmatrix} = E_{ex}\begin{bmatrix}-\sin(\theta_{er})\\ \cos(\theta_{er})\end{bmatrix} \quad (13)$$

θ_{er}, the estimated rotor position error, can be obtained using the arctan function as shown in Equation 14.

$$\theta_{er} = \tan^{-1}\left(\frac{\hat{e}_\gamma}{\hat{e}_\delta}\right) \quad (14)$$

The tracking observer, which includes a back-EMF observer, is a crucial part of sensorless FOC. If the observer output has an estimation error θ_{er}, a structure is needed to force this error to zero ($\theta_{er} = 0$) (Vidlak, 2022). This criterion can be satisfied by the PLL observer, which offers zero displacement between the calculated γδ and dq reference frames. The estimated position $\hat{\theta}_e$. and speed $\hat{\omega}_e$ are the PLL observer's outputs. The schematic of the back-EMF and tracking observer, which includes the PLL mechanism, is displayed in Figure 5.

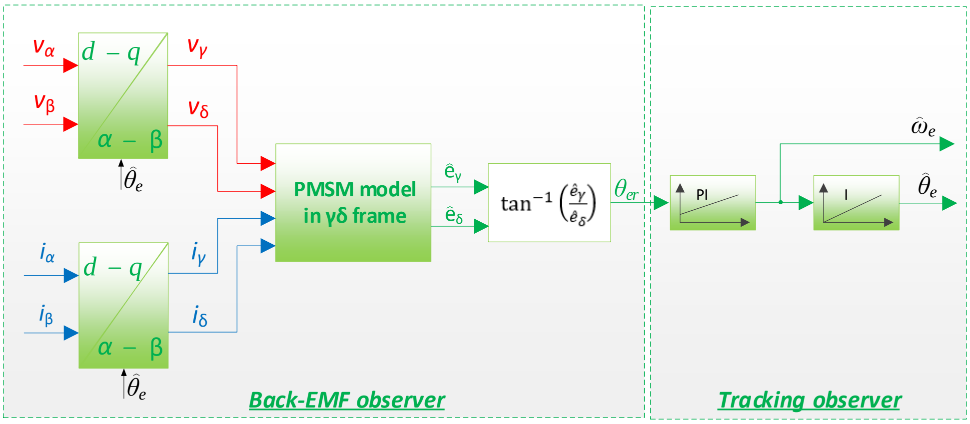

Figure 5. Diagram Of The Tracking Observer And Back-EMF Using The PLL Mechanism

4. Space Vector PWM

Three-phase systems can be transferred to two-phase planes (α-β) with a 90° phase difference between them. Space vector PWM modulation is based on the space vector representation of voltages in the (α-β) plane (Broeck et al., 1988). Additionally, space vector PWM modulation can be used to generate output voltages in three-phase voltage-source inverters by sequentially switching the basic space vectors. The three-phase voltages of the machine are represented as the space vector reference voltage (v_{ref}) in the (α-β) planes. This situation is mathematically expressed in Equation 15.

$$v_{ref} = v_\alpha + jv_\beta = (2/3)(v_a e^{j0} + v_b e^{\frac{j2\pi}{3}} + v_c e^{-\frac{j2\pi}{3}} \quad (15)$$

In classical two-level inverters, the level of the output voltage waveform consists of two levels, with each phase leg having two switches, making a total of six switches in the inverter. These switches are turned on or off sequentially throughout the period. The three-phase two-level voltage-source inverter is shown in Figure 6. The voltages v_a, v_b and v_c are applied to the stator phase windings of the IPMSM.

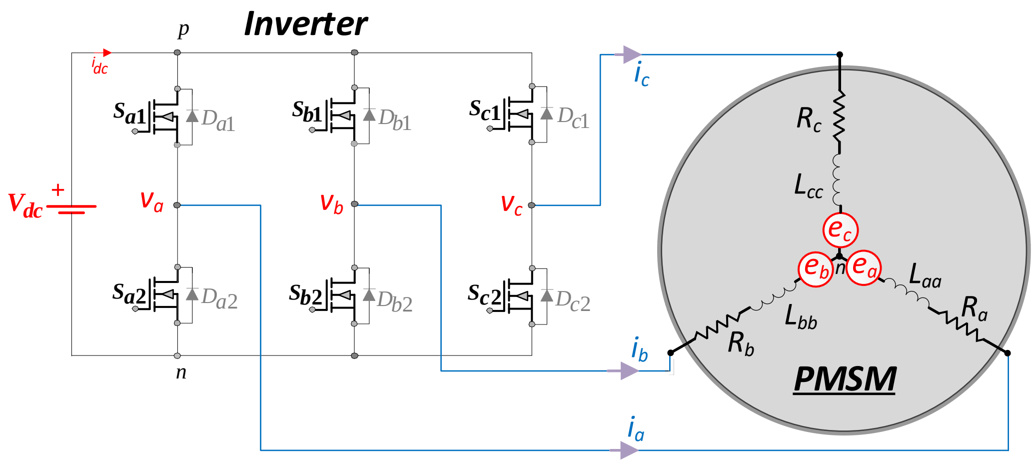

Figure 6. Three-Phase Two-Level Voltage-Source İnverter

Each phase (leg) of the inverter has two semiconductor power switches ($S_{a1} - S_{a2}$, $S_{b1} - S_{b2}$ and $S_{c1} - S_{c2}$). When one switch is on, the other must be off. The inverter can have three switching variables (a, b, and c). The total number of switching states in a two-level inverter is ($n^3 = 2^3 = 8$). In the switching states (S_{ax}, S_{bx}, S_{cx}) shown in Table 2, '1 or p' indicates the upper switch of a phase leg is on, and '0 or n' indicates the lower switch of a phase leg is on.

Table 2. Switching States Of The Two-Level Voltage-Source İnverter

Voltage Vector	Switch State					
	S_{ax}		S_{bx}		S_{cx}	
v0	0	n	0	n	0	n
v1	1	p	0	n	0	n
v2	1	p	1	p	0	n
v3	0	n	1	p	0	n
v4	0	n	1	p	1	p
v5	0	n	0	n	1	p
v6	1	p	0	n	1	p
v7	1	p	1	p	1	p

Figure 7 shows the space vector voltage representation of the two-level, three-phase voltage source inverters on the (α and β) plane.

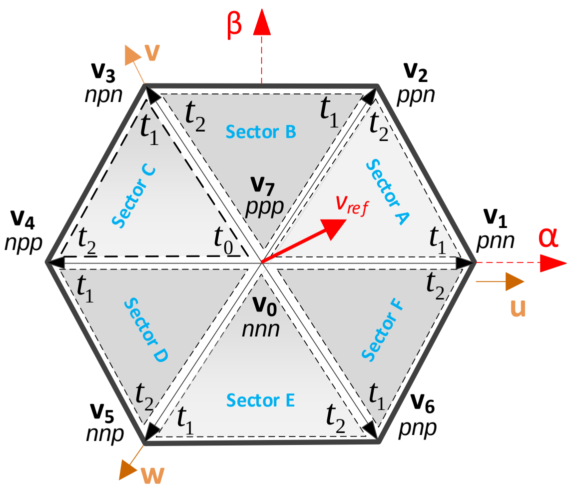

Figure 7. The Three-Phase, Two-Level İnverter's Space Vector Voltages

The reference voltage vector for Sector A is shown in Figure 8.

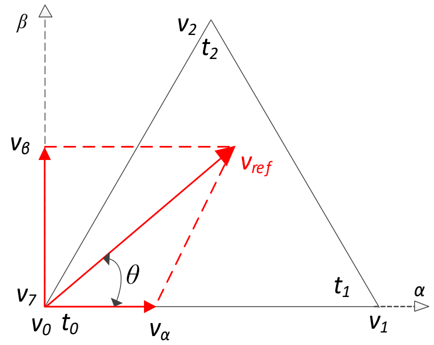

Figure 8. Reference Voltage Vector For Sector A

The durations of the voltage vectors can be found using Equations 16 and 17.

$$v_{ref}T_s = v_1t_1 + v_2t_2 + v_0t_0 \quad (16)$$

$$T_s = t_1 + t_2 + t_0 \quad (17)$$

Here, v_1, v_2, v_0 are the voltage vectors in Sector A, T_s is the sampling time, t_1, t_2, t_0 are the switching times of the voltage vectors v_1, v_2, v_0 respectively, and v_α, v_β are the real and imaginary parts of the v_{ref} voltage vector. The three-phase PWM waveforms for Sector A are shown in Figure 9. Symmetric waveforms are used for the switching sequence in each sector.

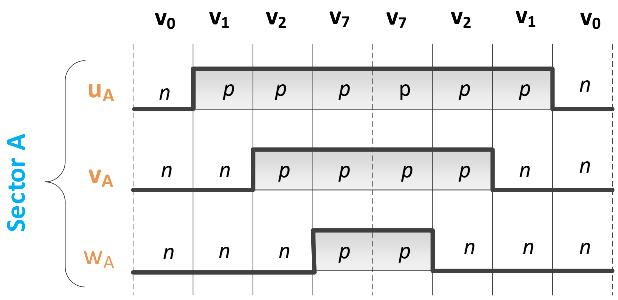

Figure 9. Three Phase PWM Waveforms Of Sector A

5. IPMSM Driver Circuit

Enhancing the effectiveness and performance of IPMSMs is largely dependent on the design and control of the motor driver. The motor driver board includes a microcontroller, power module, gate drivers, hardware protection circuits, current sensing circuits, and voltage sensing circuits. Component selection and board design directly affect the driver outputs.

5.1. Microcontroller

The performance of microcontroller-based controllers is critical in controlling the dynamics such as speed, position, or torque of electric machines (Ravigan et al., 2017). The STSPIN32F0251 microcontroller provides ADC and PWM outputs. In this study, based on a 48MHz controller frequency, a 14MHz ADC frequency and a 48MHz clock for the PWM in the APB structure were chosen. Data sampled during an ADC module sampling period is processed and used for the PWM module output. ADC and PWM must be synchronized to operate at the same speed.

The STSPIN32F0251 has six PWM modules within one counter structure. PWM techniques are commonly employed in motor control applications to regulate the output voltage's frequency and amplitude. The controller frequency, processed through the PSC (Prescaler), is applied to the motor as the switching frequency. CCR (capture compare register) and ARR (auto reload register) are used to control the PWM duty cycle.

5.2. Power Modules

The power module design, shown in Figure 10, uses the FDD86567 MOSFET from ONSEMI. The FDD86567 can handle 60V and 100A at 25°C, with an internal resistance of 3.2mΩ. Each phase uses two MOSFETs in a half-bridge configuration. During gate charging, a 12Ω resistor is used, while a 1N4148 is used during discharging.

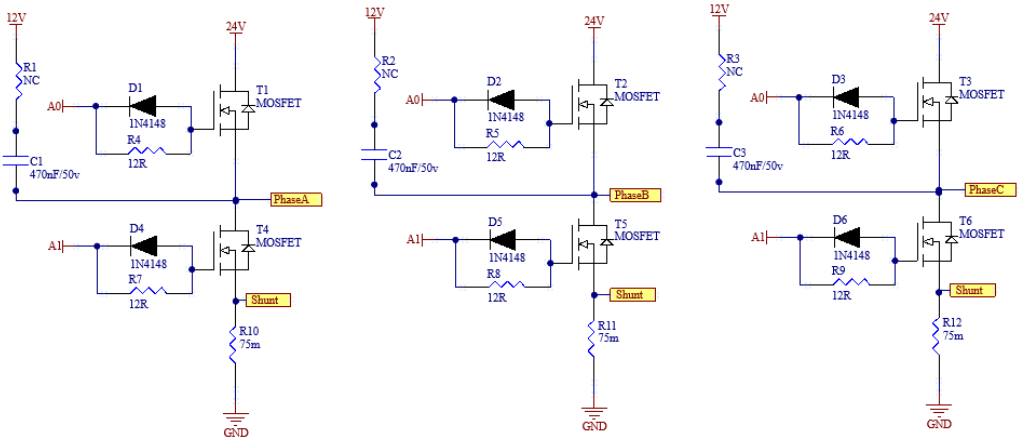

Figure 10. Power Module Design

5.3. Gate Driver Circuit

The driver circuit is a critical component that transfers control signals to the power circuit, ensuring proper switching of the power circuit. The gate drivers integrated within the STSPIN32F0251 microcontroller are used to drive the switching elements. The gate driver circuit is shown in Figure 11. The half-bridge structure control for each phase is provided by the Bootstrap method. The value of the Bootstrap capacitor directly affects the torque and voltage of the motor.

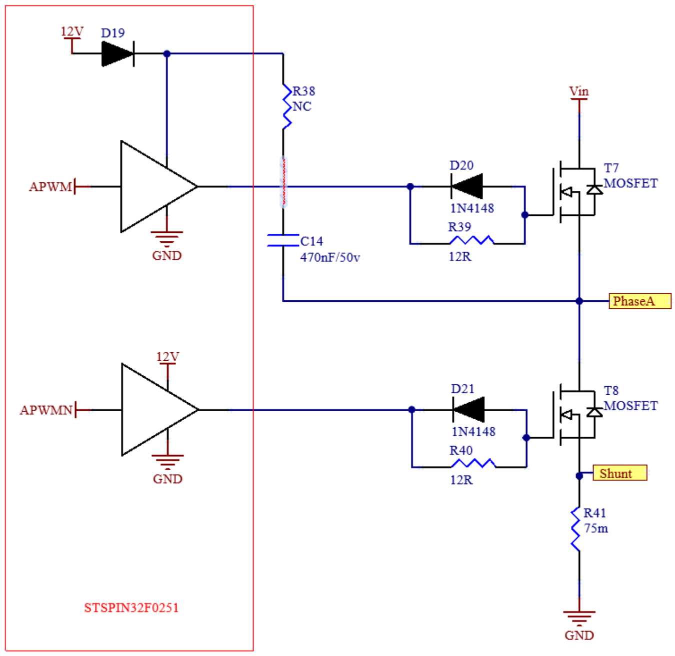

Figure 11. Gate Driver Circuit

The microcontroller contains a diode for the bootstrap structure. Externally, a Bootstrap capacitor, suitable for the motor's nominal operation, is used to keep the high side MOSFET gate voltage higher than the source voltage. This voltage difference allows the high side MOSFET to turn on.

5.4. Hardware Protection Circuits

Hardware protection circuits are designed to monitor and protect the motor's power supply. The motor controller measures the power line voltage in real-time using a voltage divider. This voltage ensures the power line voltage remains within set limits and automatically takes protective measures in low or high voltage situations.

With the temperature and voltage sensing circuits, the instantaneous bus voltage and temperature of the motor driver can be monitored through resistors. The input voltage here is one of the voltage references used. Temperature measurement applications are carried out using thermistors (NTC) placed close to the phases or switching elements. The schematics for the temperature and voltage sensing circuits are shown in Figure 12.

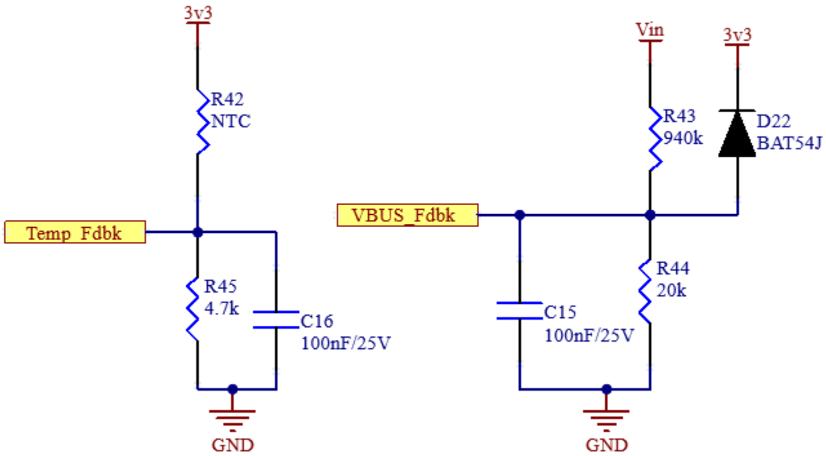

Figure 12. Temperature and Voltage Reading Circuits

Hardware protection circuits protect the motor controller from undesirable situations and potential risks in the power circuits. They safeguard the motor from potential faults such as overcurrent, overvoltage, and overheating, ensuring safe and stable operation.

5.5. Current Control Circuits

Current control circuits are designed to monitor and control the operating current of the motor. The motor driver senses the three-phase winding currents using a shunt resistor. This current value, proportional to the selected resistor tolerance and quality, can measure large currents with high accuracy and low power consumption. Thus, the motor's current values are monitored in real-time, and desired current levels are adjusted.

The voltage generated by the current passing through the shunt resistor is amplified by an opamp. The opamp structure limits and filters the current signal in the 0-3V range. Along with hardware filters, software filters are also used to process the ADC value read, and the phase current is measured. Each phase uses 75mΩ, 2W resistors for current measurement. This value is read by the microcontroller. Current parameters in the Clark Park transformation and observer are obtained. Figure 13 shows the circuit for the current sensing.

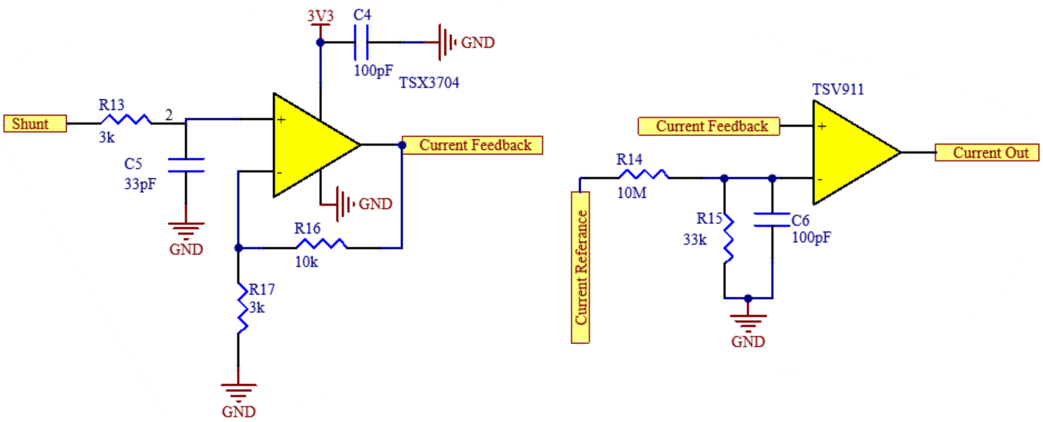

Figure 13. Current Sensing Circuit

5.6. Voltage Control Circuits

The initial back-EMF detection technique enables sensorless rotor position determination during motor startup. Zero-crossing points occur in the motor phase signal. Various hardware filters are used to read and interpret the phase voltage. The obtained value is read by the microcontroller. Voltage parameters in the Clark Park transformation and observer are obtained. The voltage sensing circuits are shown in Figure 14.

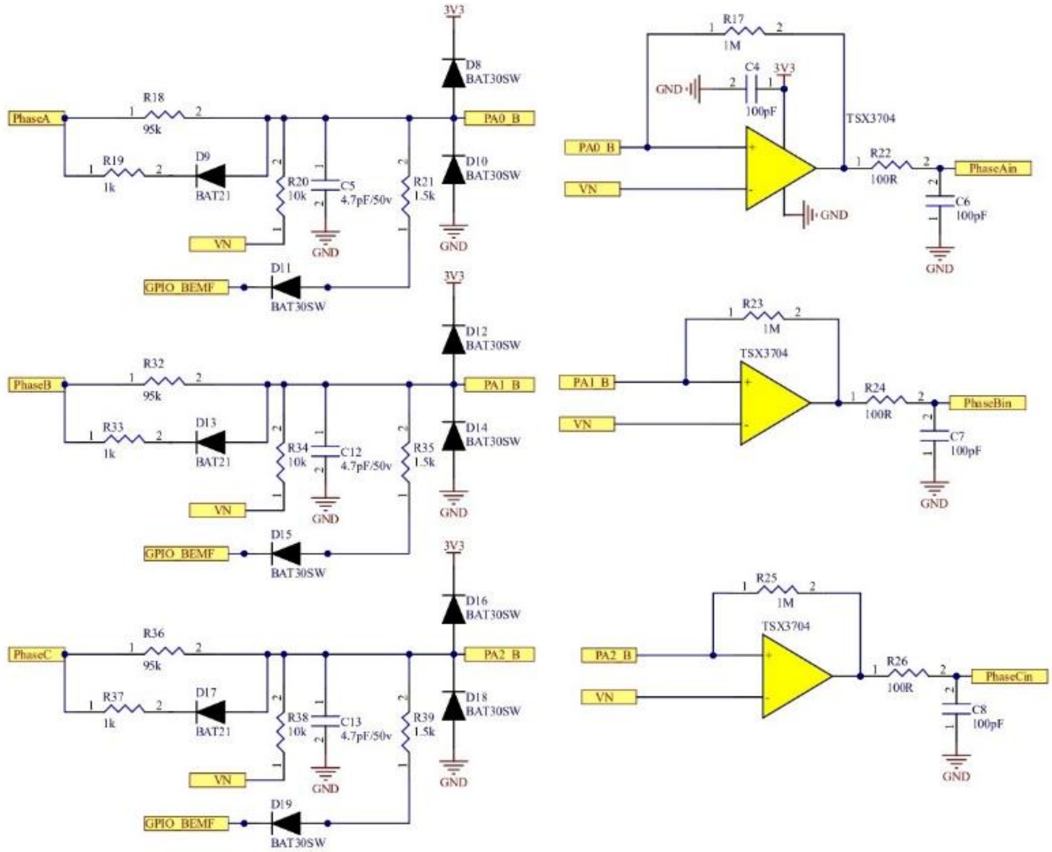

Figure 14. Voltage Sensing Circuit

The signal taken from the phase output is connected to 3V via a diode to prevent and limit interference. Here, the diodes, capacitors, and resistors applied to the input signal from the GND and 3V lines act as filters. These passive components also limit the voltage and current of the signal. The signal is filtered with the help of diodes and capacitors to receive the maximum voltage of the signal diode. The TSX3701 opamp structure amplifies it to 0-3V, making it readable by the microcontroller. The back EMF signal is detected between the motor phases. Zero crossing points are observed in this signal, and it is processed to control the phase voltage using the DGM. ADC, DGM, and other modules are initiated simultaneously with the start of the algorithm. Each phase undergoes the same processing, but the EMF signal is common to each phase. This point is one of the references used by the processor when reading analog signals.

5.7. PCB Design

The PCB layout of the motor controller prioritizes the arrangement of significant circuit units and key components. These are positioned according to the signal flow direction as indicated in the main block diagram. Main components such as the power supply and the microprocessor are given priority on the control board. The microprocessor's minimum system circuit, sampling circuit, and power supply circuit on the control board are organized separately. Additionally, the PCB design considers the problem of electromagnetic compatibility (EMC). All components are used in surface-mounted device (SMD) packages, ensuring small size, light weight, and easy storage. The TO252-DPAK package is specifically chosen for the MOSFET to gain a size advantage. In the PCB design, filter and decoupling capacitors are used to maintain the power integrity of electronic systems and limit noise.

Figure 15 shows the motor control board. In section 1 of the board, the filter circuit is located. For many applications, PI and L type filters can be preferred. At this stage, it is anticipated that the use of capacitors in addition to motor power will be sufficient. In section 2 of the board, the regulator and microcontroller circuit is located. Regulators reduce the voltage to provide power to the microcontroller and gate drives of the switching elements. In section 3 of the board, MOSFET switching elements are located within the power layer. PWM signals from the microcontroller are applied to the motor. In section 4 of the board, there is a circuit design necessary for performing the operations required for rotor position estimation via phase voltage signals. In section 5 of the board, the current sensor is located. The last two sections are used to determine the rotor position and provide the appropriate drive based on this position. Table 3 presents the sections of the motor control board.

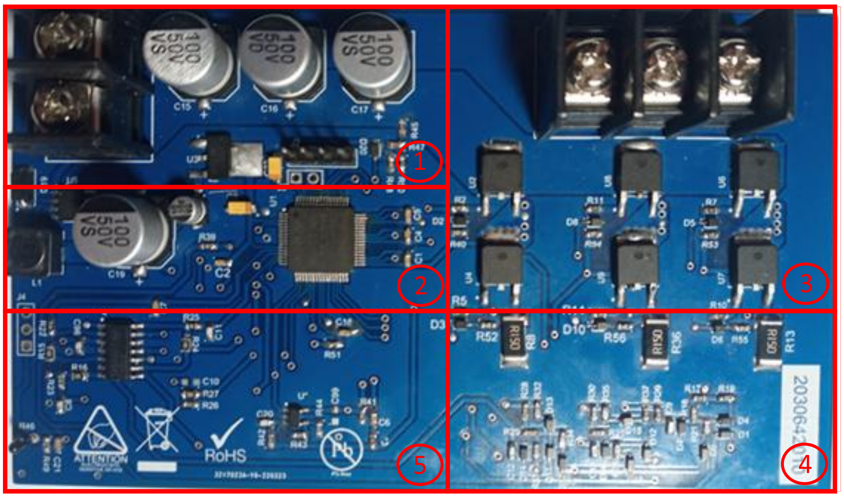

Figure 15. Motor Control Board

Table 3. Sections of the motor control board

No	Hardware
1	Filter circuit
2	Regulator circuit and MCU
3	Power layer
4	Back EMF detection circuit
5	Current sensing circuit

6. Experimental Result and Discussion

The experimental setup was designed to evaluate the motor's performance under various conditions. The torque device test of the driver encompasses a test where the torque produced by the motor under various loads is measured. The axial fan load test of the driver evaluates how the motor behaves under an axial fan load. The axial fan serves as a load to determine how the motor operates under different loads and to assess the motor's performance. During this test, the motor was operated under the axial fan load, and the torque and speed values produced by the motor under these conditions were measured. The experimental setup is shown in Figure 16. Tests were conducted on the torque device and on the axial fan for field applications for the IPMSM driver. Table 4 lists the equipment used in the experimental setup.

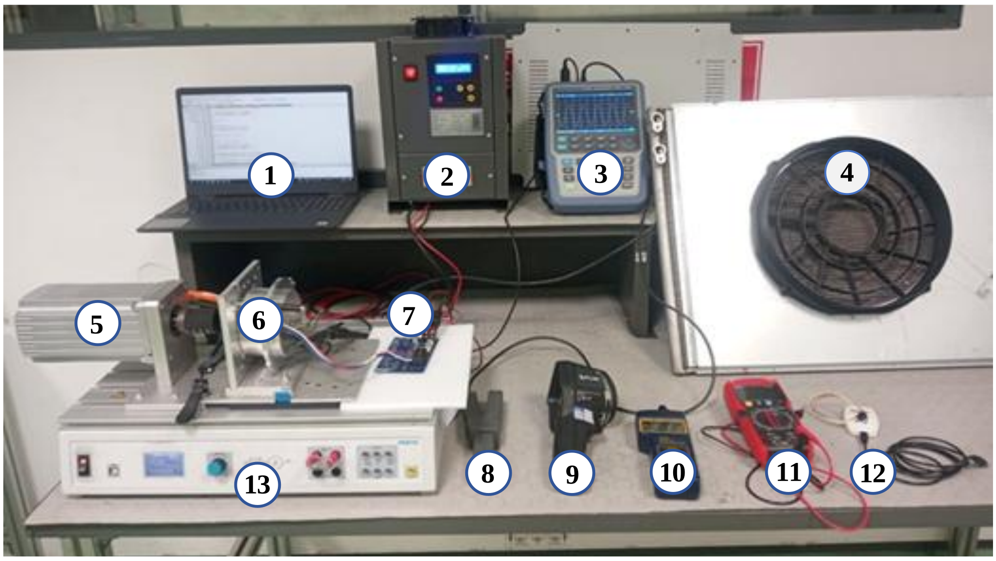

Figure 16. Experiment Setup

Table 4. Equipment Used İn Experiment Setup System

No	Hardware
1	Computer
2	Power Supply
3	Oscilloscope
4	Axial Fan
5	Torque Meter
6	Interior Permanent Magnet Synchronous Motor (IPMSM)
7	IPMSM Control Board
8	Current Probe
9	Thermal Camera
10	Tachometer
11	Multimeter
12	Programmer
13	TP 1410 Motor Test Platform

The Festo TP1410 Motor Test Platform and DriveLab software shown in the experimental setup allow for the examination of electric motors under various loads. This setup supports the automatic recording of motor characteristics, determination of static load parameters, and simulation of different load models. Specifically, it can start with load configurations that include various load models such as pumps, fans, and dynamic loads. This enables a detailed analysis of motor performance. Typical tests involve starting from the nominal load to the maximum load and the instantaneous engagement of different loads. During this process, key data such as motor speed, source current (i_{dc}), and applied torque can be monitored. Figure 17 shows the speed, torque, and current graphs.

In this study, a fan load was selected on the load device, taking fan load applications as a reference. In fan applications, the motor starts together with the fan load. Therefore, the tests started under load, and the minimum torque was determined. In fan applications, proportional speed control or step control is performed. In this study, the motor was tested at three different speed values: 1000 rpm during the (2-12)s time interval, 2000 rpm during the (12-22)s time interval, and 3000 rpm during the (22-35)s time interval. The nominal fan load was 0.3 Nm, and the maximum fan load was 0.7 Nm. During the test, the motor operating under a 0.3 Nm load was exposed to a maximum load of 0.7 Nm at 1000 rpm during the (5-10)s time interval, at 2000 rpm during the (15-20)s time interval, and at 3000 rpm during the (25-30)s time interval. During the process of adding and removing loads, instantaneous current and speed data were obtained in Excel format using the Festo DriveLab application. The obtained Excel data was then plotted using Matlab.

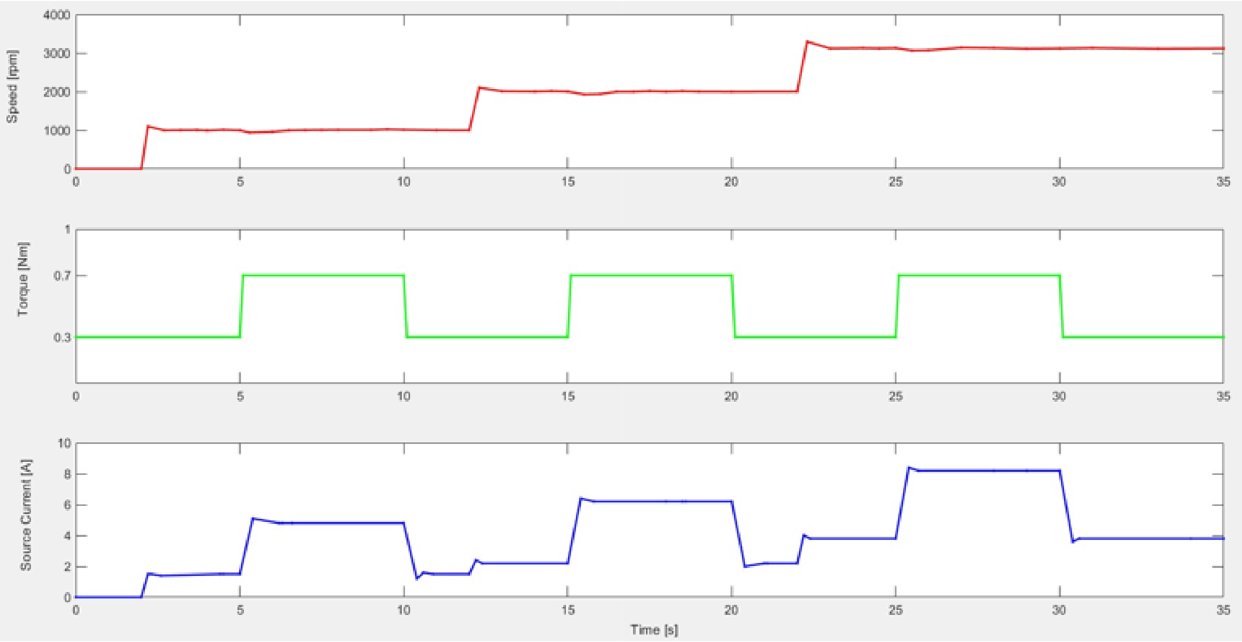

Figure 17. Experimental Results Of IPMSM; A) Speed B) Torque C) Source Current

5. Conclusions

In this study, an Interior Permanent Magnet Synchronous Motor (IPMSM) was used for automotive climate control systems due to its low cost, high starting torque, fast response times, and high dynamic performance. To enhance the motor's performance and efficiency, a motor driver design was implemented. The motor driver board includes a microcontroller, power module, gate drivers, hardware protection circuits, current reading circuits, and voltage reading circuits. The design and component selection of the motor driver board directly affect its performance. Besides the motor driver design, control methods are also crucial for the motor's performance. In this study, a Luenberger-type sensorless control method was employed. The motor was powered by a space vector PWM-based two-level inverter. Experimental results showed that IPMSMs exhibit high performance for industrial fan applications.

Acknowledgments

The authors would like to express their gratitude to Kormas Electric Motor for their unwavering support during the design and production of this study.

Conflict of Interest

Yazarlar tarafından herhangi bir çıkar çatışması beyan edilmemiştir. No conflict of interest was declared by the authors.

References

Abo-Khalil, A. G., Eltamaly, A. M., Alsaud, M. S., Sayed, K., & Alghamdi, A. S. (2021). Sensorless control for PMSM using model reference adaptive system. International Transactions on Electrical Energy Systems, 31(2), e12733.

Aydogmus, O., & Sünter, S. (2012). Implementation of EKF based sensorless drive system using vector controlled PMSM fed by a matrix converter. International Journal of Electrical Power & Energy Systems, 43(1), 736-743.

Borsje, P., Chan, T. F., Wong, Y. K., & Ho, S. L. (2005, May). A comparative study of Kalman filtering for sensorless control of a permanent-magnet synchronous motor drive. In IEEE International Conference on Electric Machines and Drives, 2005. (pp. 815-822).

Broeck HW, Skudelny HC, Stanke GV. "Analysis and realization of a pulsewidth modulator based on voltage space vectors". IEEE Transactions on Industry Applications, 24 (1), 142-150, 1988.

Elmas, C., & Ustun, O. (2008). A hybrid controller for the speed control of a permanent magnet synchronous motor drive. Control Engineering Practice, 16(3), 260-270.

Genduso, F., Miceli, R., Rando, C., & Galluzzo, G. R. (2010). Back EMF sensorless-control algorithm for high-dynamic performance PMSM. IEEE Transactions on Industrial Electronics, 57(6), 2092-2100.

Güngör, B., Özgenel, M.C., & Demirbaş, Ş. (2010). Dynamic analysis of vector controlled permanent magnet synchronous motor driven with SPWM inverter. Journal of the Faculty of Engineering & Architecture of Gazi University, 25(3), 569-577.

Huang, Q., Huang, Q., Guo, H., & Cao, J. (2023). Design and research of permanent magnet synchronous motor controller for electric vehicle. Energy Science & Engineering, 11(1), 112-126.

Jung, W. S., Lee, H. K., Lee, Y. K., Kim, S. M., Lee, J. I., & Choi, J. Y. (2023). Analysis and Comparison of Permanent Magnet Synchronous Motors According to Rotor Type under the Same Design Specifications. Energies, 16(3), 1306.

Kanchan RS, Baiju MR, Mohapatra KK, Ouseph PP, Gopakumar K. "Space vector PWM signal generation for multilevel inverters using only the sampled amplitudes of reference phase voltages". Electric Power Applications, IEE Proceedings, 152 (2), 297-309, 2005.

Kim, S. I., Im, J. H., Song, E. Y., & Kim, R. Y. (2016). A new rotor position estimation method of IPMSM using all-pass filter on high-frequency rotating voltage signal injection. IEEE Transactions on Industrial Electronics, 63(10), 6499-6509.

Krishnan, R. (1987). Selection criteria for servo motor drives. IEEE Transactions on Industry Applications, IA-23(2), 270-275.

Luo, X., Tang, Q., Shen, A., & Zhang, Q. (2015). PMSM sensorless control by injecting HF pulsating carrier signal into estimated fixed-frequency rotating reference frame. IEEE Transactions on Industrial Electronics, 63(4), 2294-2303.

Murakami, H., Honda, Y., Kiriyama, H., Morimoto, S., & Takeda, Y. (1999, October). The performance comparison of SPMSM, IPMSM and SynRM in use as air-conditioning compressor. In Conference Record of the 1999 IEEE Industry Applications Conference. Thirty-Forth IAS Annual Meeting (Cat. No. 99CH36370) (Vol. 2, pp. 840-845). IEEE.

Ni, R., Xu, D., Blaabjerg, F., Lu, K., Wang, G., & Zhang, G. (2017). Square-wave voltage injection algorithm for PMSM position sensorless control with high robustness to voltage errors. IEEE Transactions on Power Electronics, 32(7), 5425-5437.

Noguchi, T. (2007). Trends of permanent-magnet synchronous machine drives. IEEJ Transactions on Electrical and Electronic Engineering, 2(2), 125-142.

Piippo, A., Hinkkanen, M., & Luomi, J. (2009). Adaptation of motor parameters in sensorless PMSM drives. IEEE Transactions on Industry Applications, 45(1), 203-212.

Quang, N. K., Hieu, N. T., & Ha, Q. P. (2014). FPGA-based sensorless PMSM speed control using reduced-order extended Kalman filters. IEEE transactions on Industrial Electronics, 61(12), 6574-6582.

Rahman, M. A., Milasi, R. M., Lucas, C., Araabi, B. N., & Radwan, T. S. (2008). Implementation of emotional controller for interior permanent-magnet synchronous motor drive. IEEE Transactions on Industry Applications, 44(5), 1466-1476.

Saleh, S. A., Ozkop, E., Nahid-Mobarakeh, B., Rubaai, A., Muttaqi, K. M., & Pradhan, S. (2023). Survivability-Based Protection for Electric Motor Drive Systems-Part II: Three Phase Permanent Magnet Synchronous Motor Drives. IEEE Transactions on Industry Applications. 59(3), 2760 – 2771.

Schroedl, M. (1996, October). Sensorless control of AC machines at low speed and standstill based on the" INFORM" method. In IAS'96. Conference Record of the 1996 IEEE Industry Applications Conference Thirty-First IAS Annual Meeting (Vol. 1, pp. 270-277).

Sen, P. C. (1990). Electric motor drives and control-past, present, and future. IEEE Transactions on Industrial Electronics, 37(6), 562-575.

Song, X., Fang, J., Han, B., & Zheng, S. (2016). Adaptive compensation method for high-speed surface PMSM sensorless drives of EMF-based position estimation error. IEEE Transactions on Power Electronics, 31(2), 1438-1449.

Ullah, K., Guzinski, J., & Mirza, A. F. (2022). Critical review on robust speed control techniques for permanent magnet synchronous motor (PMSM) speed regulation. Energies, 15(3), 1235.

Vidlak, M., Makys, P., & Gorel, L. (2022). A Novel Constant Power Factor Loop for Stable V/f Control of PMSM in Comparison against Sensorless FOC with Luenberger-Type Back-EMF Observer Verified by Experiments. Applied Sciences, 12(18), 9179.

Volpato Filho, C. J., Xiao, D., Vieira, R. P., & Emadi, A. (2021). Observers for high-speed sensorless pmsm drives: Design methods, tuning challenges and future trends. IEEE Access, 9, 56397-56415. Digital Object Identifier 10.1109/ACCESS.2021.3072360.

Wang, G., Valla, M., & Solsona, J. (2019). Position sensorless permanent magnet synchronous machine drives—A review. IEEE Transactions on Industrial Electronics, 67(7), 5830-5842. Digital Object Identifier 10.1109/TIE.2019.2955409.

Wang, Q., Wang, S., & Chen, C. (2019). Review of sensorless control techniques for PMSM drives. IEEJ Transactions on electrical and electronic engineering, 14(10), 1543-1552.

Wang, Z., Lu, K., & Blaabjerg, F. (2012). A simple startup strategy based on current regulation for back-EMF-based sensorless control of PMSM. IEEE Transactions on Power Electronics, 27(8), 3817-3825.

Yan, H., Xu, Y., Cai, F., Zhang, H., Zhao, W., & Gerada, C. (2018). PWM-VSI fault diagnosis for a PMSM drive based on the fuzzy logic approach. IEEE Transactions on Power Electronics, 34(1), 759-768.

Zhang, G., Wang, G., & Xu, D. (2017). Saliency-based position sensorless control methods for PMSM drives-A review. Chinese Journal of Electrical Engineering, 3(2), 14-23.

Zhang, H., Zhang, G., Shen, W., Wang, G., & Xu, D. (2020, November). Fundamental PWM Excitation Based Low-Speed Sensorless Control Method for PMSM Drives. In 2020 15th IEEE Conference on Industrial Electronics and Applications (ICIEA) (pp. 833-838).

Zhang, X., Li, H., Yang, S., & Ma, M. (2017). Improved initial rotor position estimation for PMSM drives based on HF pulsating voltage signal injection. IEEE Transactions on Industrial Electronics, 65(6), 4702-4713.

Zhang, Z. (2022). Sensorless Control of Synchronous Machines Using Fundamental Back-EMF Voltage-A Review. IEEE Transactions on Power Electronics, 37(9), 10290-10305.